Cellulose Nanocrystal-Assisted Dispersion of Luminescent Single-Walled Carbon Nanotubes for Layer-by-Layer Assembled Hybrid Thin Films

ARTICLE *in* LANGMUIR · AUGUST 2012

Impact Factor: 4.46 · DOI: 10.1021/la302077a · Source: PubMed

6 AUTHORS, INCLUDING:

Céline Moreau
French National Institute for Agricultural Rese…
33 PUBLICATIONS **255** CITATIONS
SEE PROFILE

Bertoncini Patricia
University of Nantes
28 PUBLICATIONS **407** CITATIONS
SEE PROFILE

Olivier Chauvet
University of Nantes
138 PUBLICATIONS **4,436** CITATIONS
SEE PROFILE

Langmuir

Article

pubs.acs.org/Langmuir

Cellulose Nanocrystal-Assisted Dispersion of Luminescent Single-Walled Carbon Nanotubes for Layer-by-Layer Assembled Hybrid Thin Films

Christophe Olivier,*[,†,‡] Céline Moreau,[†] Patricia Bertoncini,[‡] Hervé Bizot,[†] Olivier Chauvet,[‡] and Bernard Cathala[†]

[†]INRA-BIA, UMR 1268 Biopolymères, Interactions et Assemblages, 44316 Nantes, France.

[‡]IMN, UMR 6502 CNRS-Université de Nantes, 44322 Nantes, France

Supporting Information

ABSTRACT: Highly stable single-walled carbon nanotube (SWNT) dispersions are obtained after ultrasonication in cellulose nanocrystal (CN) aqueous colloidal suspensions. Mild dispersion conditions were applied to preserve the SWNT length in order to facilitate the identification of hybrid objects. This led to a moderate dispersion of 24% of the SWNTs. Under these conditions, atomic force microscopy (AFM) and transmission electron microscopy (TEM) experiments succeeded in demonstrating the formation of hybrid particles in which CNs are aligned along the nanotube axis by a self-assembly process. These SWNT/CN dispersions are used to create multilayered thin films with the layer-by-layer method using polyallylamine hydrochloride as a polyelectrolyte. Homogeneous films from one to eight bilayers are obtained with an average bilayer thickness of 17 nm. The presence of SWNTs in each bilayer is attested to by characteristic Raman signals. It should be noted that these films exhibit a near-infrared luminescence signal due to isolated and well-separated nanotubes. Furthermore, scanning electron microscopy (SEM) suggests that the SWNT network is percolating through the film.

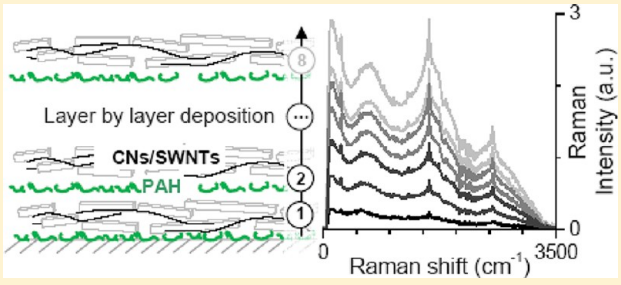

1. INTRODUCTION

Self-assembled thin films such as self-assembled monolayers (SAM),[1] Langmuir−Blodgett (LB)[2] films, and layer-by-layer (LbL)[3] assemblies represent a very active area of research because of the large panel of applications for a wide range of fields, including electronic devices[4] and biomedicine.[5] Among all of the self-assembly techniques reported in the literature, the LbL approach introduced by Decher et al.[3] has attracted a great amount of interest because of its simplicity and versatility.[6] On the basis of the alternate adsorption of oppositely charged polyelectrolytes, this method is available for a wide variety of materials and substrates and allows, in particular, accurate control of the film structure on the nanoscale level.[7,8] The method was first applied to synthetic polyelectrolytes such as poly(allylamine hydrochloride) (PAH) and polystyrene sulfonate (PSS)[9] that have been assembled with poly(phenylene vinylene) (PPV) for light-emitting diodes,[10] azo-benzene for nonlinear optics,[11] and biomolecules for drug release[12] and biosensing.[13] LbL assembly is also appropriate for the deposition of nanosized components such as nanoparticles[14] and carbon nanotubes,[15] thus leading the way in the preparation of multifunctional films. Biosourced nano-objects[16−20] were also incorporated into such films, yielding environmentally friendly multilayered thin films with optimized properties.

Cellulose nanocrystals (CNs) have received a considerable amount of attention because they are original bionanorods with unusual mechanical characteristics and a large panel of interactions.[21] CNs are derived from cellulose fibrils that are composed of linear cellulose chains of $\beta(1-4)$-D-glucose residues that self-assemble in highly crystalline fibrils. In vivo slender cellulose microfibrils are combined with other biomacromolecules to form supramolecular assemblies (i.e., plant cell walls), where they act as a reinforcer. Cellulose nanocrystals, also referred to as cellulose whiskers, are single-crystalline rods obtained from the harsh sulfuric acid hydrolysis of microfibrils, with a cross-section of between 3 and 20 nm and a length of between 100 nm and several micrometers, depending on their biological origin.[22] The mechanical dissociation of cellulose whiskers leads to stable colloidal suspensions as a result of the sulfate charges introduced onto the crystal surface during hydrolysis. The presence of these sulfated charged groups at the CN surface also makes them suitable for interaction with polycations to obtain multilayered thin films, as demonstrated for the first time by Kotov et al.[17] Later studies demonstrated that multilayered thin films based

Received: December 19, 2011
Revised: August 2, 2012
Published: August 6, 2012

on CNs can be an efficient platform for the creation of innovative coatings. For example, Podsiadlo et al.[8] reported the fabrication of tunicate CN-based LbL films that show strong antireflective properties as a result of the high aspect ratio of the tunicin nanorods and a nanoporous structure. Later on, films obtained from cotton CNs were found to exhibit other optical properties because of dense surface packing that leads to the appearance of color as a result of interference phenomena.[23] Similar optical properties were also demonstrated on films obtained from microfibrillated cellulose/polyelectrolytes[24] as well as on thin films made from xyloglucan and cotton whiskers.[25] In the latter case, the optical properties of the films were used to develop a highly efficient method for enzyme detection.[20] Thus, in order to develop new potential applications based on the LbL CN coating, we aimed to investigate the incorporation of SWNTs to form organic/inorganic hybrid films.

Among various functional nanoscale objects, single-walled carbon nanotubes (SWNTs) are promising candidates for emerging materials because of their unique physical, chemical, and mechanical properties.[26] However, SWNTs are hydrophobic, and their dispersion in water is a critical step in their use in a biological medium. One dispersion strategy in an aqueous medium consists of the oxidation of the graphitic surface of the nanotubes[27] or chemical grafting[28] to introduce repulsive interactions or steric hindrance between nanotubes in order to achieve colloidal stability. However, SWNT properties can be severely altered by the chemical modification of their surface.[29] Another approach is based on noncovalent functionalization. In this case, SWNTs are debundled by an ultrasonic treatment, and the stability of the dispersion in water is then ensured by the use of surfactant molecules, polymers, or biopolymers.[30] Both strategies were used to prepare SWNT multilayered thin films using the LbL approach. For example, Mamedov et al.[15] incorporated oxidized SWNTs into polymer films, whereas Zhang et al.[31] reported the preparation of LbL films by dispersing SWNTs using sodium dodecyl sulfate. The resulting films exhibited enhanced mechanical properties with a homogeneous distribution of SWNTs in the films and efficient charge transfer from SWNTs to the polymer matrix. Since this pioneering work, SWNT multilayered films prepared by the LbL method from surfactant-, polymer-, or biopolymer-based SWNT dispersions represent a very active area of research with applications to transparent electrodes,[32] photoconversion devices,[33] physical sensors,[34] biosensors,[35] antimicrobial coatings,[36] and drug release,[37] for example.

The aim of this work was to develop cellulose-based multifunctional thin films with specific properties arising from both SWNTs and CNs. We report the dispersion of SWNTs by cellulose nanocrystals and the subsequent use of CN/SWNT aqueous dispersions for the development of multilayered thin films. Stable dispersions of SWNTs were obtained by sonication of the SWNTs in a CN aqueous colloidal suspension. The characterization by optical spectroscopy and imaging techniques suggests that SWNTs and CNs are associated in hybrid nano-objects where the CNs are aligned along the tube axis and the hydrophobic interaction is proposed to be the underlying force for this self-assembly process. To the best of our knowledge, this association has never been reported before and leads to new opportunities to use SWNTs in aqueous media by taking advantage of the self-assembly properties of CNs. As a proof of concept of these new opportunities, SWNTs were successfully incorporated into multilayered films by the LbL method as demonstrated by Raman scattering experiments. Quite unexpectedly, these films exhibit near-infrared luminescence due to isolated SWNTs. This illustrates the possibility of creating multifunctional multilayered thin films that combine the properties of SWNTs and CNs.

2. EXPERIMENTAL SECTION

a. Preparation of Cellulose Nanocrystal Suspensions. Cellulose nanocrystals were extracted from cotton linters using a technique adapted from Dong et al.[38] Thirty grams of cotton linters was added to 260 mL of 64% sulfuric acid (H_2SO_4) at 60 °C and stirred for 30 min. The acid hydrolysis was stopped by diluting the mixture 10-fold with distilled water. The mixture was further centrifuged (10 000 rpm, 10 min), washed, and sonicated until a stable colloidal solution was obtained. The suspension was then filtered through a fritted glass funnel (por. 1). The remaining acid and ions were removed by dialysis and treatment with an exchange resin. Sodium azide (0.01%) was added for storage. During the hydrolysis process, some hydroxyl groups from the cellulose crystal surface are replaced by negatively charged sulfate groups, inducing repulsive electrostatic interactions between the whiskers that are responsible for the colloidal stability of the whisker suspension. A CN dispersion was used at [CN] = 20 g/L and pH 4.

The quantity of charges on the CN surface was measured by conductometric titration with a 10 mM NaOH solution performed on a TIM900 titration manager and a CDM230 conductivity meter equipped with a CDC749 conductivity cell. A surface charge density of 0.5 e/nm^2 was found.

b. Preparation of SWNT/CN Dispersions. The concentration of cellulose nanocrystals in suspension was adjusted to 20 g/L before adding SWNTs. One milligram of HiPco SWNTs (Unidym, batch P0261) was predispersed in 4 mL of a CN aqueous suspension by cup horn sonication (5 W, 20 kHz) for 30 min. This preparation was separated into two fractions (2 mL each) and sonicated again for 30 min (5 W, 20 kHz). The solution temperature was maintained at 10 °C during sonication. After centrifugation under the mild conditions (8700 rpm) of aqueous preparation, large SWNT bundles were precipitated and the supernatant/dispersion was removed for subsequent characterization.

c. Multilayer LbL Film Preparation. The LbL films were prepared using the dipping procedure. The multilayered films were deposited on silicon wafers for scanning electron microscopy (SEM), atomic force microscopy (AFM), and thickness measurements and on glass substrates for optical measurements. The substrates were first cleaned in a piranha solution (7:3 v/v H_2SO_4/H_2O_2) and rinsed with distilled water. Poly(allylamine hydrochloride) (M_w 120 000−200 000 g/mol; Sigma-Aldrich) solution was used at 4 g/L in a 0.1 M MES buffer at pH 4.5 [2(*N*-morpholino)ethanesulfonic acid] with the addition of 1 M NaCl. The construction of the films is based on alternate layer adsorption from polycationic PAH solution and from CN or SWNT/CN dispersion as the anionic polyelectrolyte. One layer is obtained as follows: (i) dipping the substrate in PAH or SWNT/CN solution for 1 min; (ii) rinsing in water repeatedly; and (iii) drying the surface in a stream of nitrogen. Multilayered films from one to eight bilayers (PAH− SWNTs/CNs) or (PAH−CNs) were independently fabricated according to this procedure.

d. Optical Spectroscopy. Raman scattering spectra were obtained with an excitation energy of 1.16 eV (1064 nm, laser power = 30 mW) using a Bruker RFS 100 FT-Raman spectrometer. Photoluminescence spectra were collected from the front-face geometry of the samples with a Jobin-Yvon Fluorolog spectrometer using a xenon lamp as an excitation source and an InGaAs IR detector (427C-AU Horiba). The excitation wavelength was fixed at 650 nm.

e. Profilometry Measurements. Film thicknesses were obtained with a stylus-based mechanical profilometer from Veeco Dektak-8 by measuring the depth of a scratch made with a razor blade on the film surface. The tip that was used had a radius of 2.5 μm, and the contact

force was 2 mg. Accuracy was ensured by averaging measurements from six different regions of the film.

f. Imaging Techniques. *i. Transmission Electron Microscopy (TEM).* Twenty microliters of a CN suspension or a SWNT/CN dispersion previously diluted 40-fold was deposited on freshly glow-discharged carbon-coated electron microscope grids (200 mesh, Delta Microscopies, France) for 2 min, and the excess water was removed by blotting. The sample was then immediately negatively stained with uranyl acetate solution (2% w/v) for 2 min and dried after blotting at 40 °C just before observation. The grids were observed with a Jeol JEM 1230 TEM at 80 kV. Pristine SWNTs were observed on a Hitachi HNAR 9000 at 300 kV.

ii. Atomic Force Microscopy (AFM) . To analyze the morphology of isolated CNs or SWNT/CN hybrids, a CN suspension or SWNT/CN dispersion was diluted 40-fold and then deposited on a silicon wafer using the layer-by-layer procedure. Briefly, after the substrate was cleaned, the first PAH layer was adsorbed before the SWNT/CN layer. The deposition time for this second layer was as short as possible. As a result, the nanohybrids were highly dispersed (about 1 per 100 μm^2) on a rough PAH layer. In the first set of experiments, images were recorded in air on a dried sample with a Multimode Nanoscope IIIA scanning probe microscope (Digital Instruments, Santa Barbara, CA, USA) operating in tapping mode using silicon tips (NCHR, Nanosensors). In a second set of experiments, images were recorded in ultrapure water with a Nanowizard II AFM (JPK Instruments AG, Berlin, Germany) using silicon nitride tips (OTR4, Bruker AFM probes). Images were taken in alternate contact mode with very low driven amplitudes and scan rates of <0.5 Hz. The height of features in the AFM images was analyzed using WSXM software routines.[39]

iii. Scanning Electron Microscopy (SEM). Images of the SWNT/CN films were obtained using a JEOL JSM 7600 F microscope operating at 10 kV.

All images presented (TEM, AFM, and SEM) are shown as captured.

3. RESULTS AND DISCUSSION

The incorporation of SWNTs in multilayered CN films prepared using the LbL dipping technique requires their dispersion in an aqueous polyelectrolyte solution. A non-covalent functionalization method is preferable for preserving SWNT properties. An aqueous dispersion of SWNTs and their subsequent use in LbL assembly have been reported in the presence of surfactants[31] or conventional polyelectrolytes such as poly(sodium 4-styrene sulfonate) (PSS)[40] or biomolecules such as glucose oxidase[35] and RNA.[41] In this study, to avoid the surfactant-assisted technique, the direct sonication of SWNTs in a cellulose nanocrystal suspension was used. The sonication procedure, which may be responsible for the cutting and doping of the SWNTs, was carried out under soft conditions. The CNs were found to disperse SWNTs in aqueous media effectively, yielding a black solution that was stable over several months (photograph in Figure 1). The concentration of SWNTs in the dispersion was evaluated by measuring the absorbance of the dispersion at 891 nm where the optical spectrum is not affected by the cellulose signal. Using an extinction coefficient of the SWNT dispersion at this wavelength of 2.14 mL/mg mm,[42] we found an SWNT concentration of about 0.06 mg/mL in the dispersion. This means that the SWNT/CN mass ratio is [SWNT]/[CN] = 0.0028 in this dispersion. Higher SWNT/CN mass ratios of up to 0.15 have been obtained by decreasing the initial CN concentration. However, with the aim of preparing layer-by-layer films, we have maintained our initial CN concentration at 20 g/L in order to respect the efficient parameters found in the literature. The efficiency of the dispersion process is obtained by dividing the initial SWNT concentration ([$SWNT_0$] = 0.25 mg/mL) by the concentration after sonication and centrifugation [SWNT]. It was observed that the CNs are able to stabilize [SWNT]/[$SWNT_0$] = 24% of the suspended SWNTs under these soft sonication conditions. Higher dispersion yields of up to 65% can be obtained by increasing the sonication time and power, but these sonication conditions are found to cut and damage the SWNTs. Thus, soft sonication conditions were used in this study in order to keep the SWNTs intact, to preserve their physical properties, and to facilitate the distinction between the CNs and SWNTs in microscopic investigations. For the sake of comparison, Gilman et al.[42] reported approximately 40 and 50% of suspended SWNTs in chitosan and carboxymethyl cellulose dispersions, respectively.

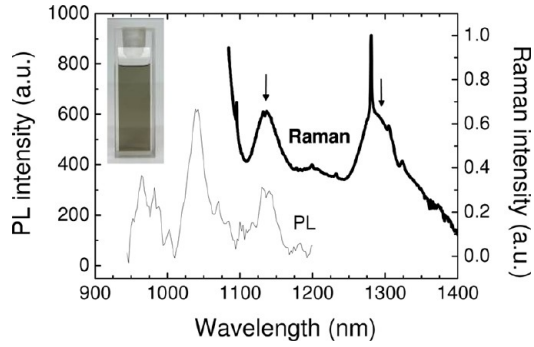

Figure 1. Raman scattering (bold line) and photoluminescence (thin line) spectra of the SWNT/CN dispersion obtained at excitation wavelengths of 1064 and 650 nm, respectively. A photograph of the SWNT/CN dispersion is displayed in the top left corner.

a. Optical Properties of SWNT/CN Dispersions. Figure 1 shows the Raman scattering (bold line) and photoluminescence (thin line) spectra of the SWNT/CN dispersion obtained at excitation wavelengths of 1064 and 650 nm, respectively. To compare both spectra, the Raman shift is converted to an absolute emission wavelength. We determined that the Raman signal of cellulose is not observable under these conditions. Sharp Raman peaks are observed at Raman shifts of ~220 and ~1600 cm^{-1} (1095 and 1280 nm wavelengths, respectively). They are due to the SWNTs' Raman-active radial breathing mode (RBM) and tangential mode (G-band), respectively.[43] This shows that the SWNTs are still present in the dispersion after centrifugation, and because there is no sedimentation, it also reveals that CNs act as stabilizers of SWNTs in aqueous solution. The Raman spectrum also displays broad peaks close to 1140 and 1290 nm. These peaks arise from the NIR emission (luminescence) of semiconducting SWNTs. They are more easily observed in the photoluminescence (PL) spectrum shown in Figure 1. For technical reasons, we were not able to observe PL over 1200 nm, but the luminescence peak at 1140 nm is easily observed in both the Raman scattering and PL spectra. As reported by O Connell et al.,[44] the specific NIR luminescence of the SWNTs attests to the presence of well-isolated semiconducting SWNTs in the dispersion and/or very small bundles of SWNTs. According to Bachilo et al.,[45] the luminescence peaks observed at 966, 1042, and 1138 nm can be assigned to (8.3), (7.5), and (7.6) semiconducting isolated SWNTs, respectively. This observation definitively suggests that CNs interact with the SWNTs in the dispersion, thus allowing the stabilization of isolated tubes.

b. SWNT/CN Complex: Morphology and Interactions. The optical properties of the dispersion suggest that an

dx.doi.org/10.1021/la302077a | *Langmuir* 2012, 28, 12463−12471

interaction exists between the CNs and the SWNTs. It is thus relevant to investigate a possible self-assembly of SWNTs and CNs by probing the morphology of these nano-objects using TEM and AFM.

Figure 2 shows TEM images from pristine SWNTs and individual CN dispersions as reference images (Figure 2a,b)

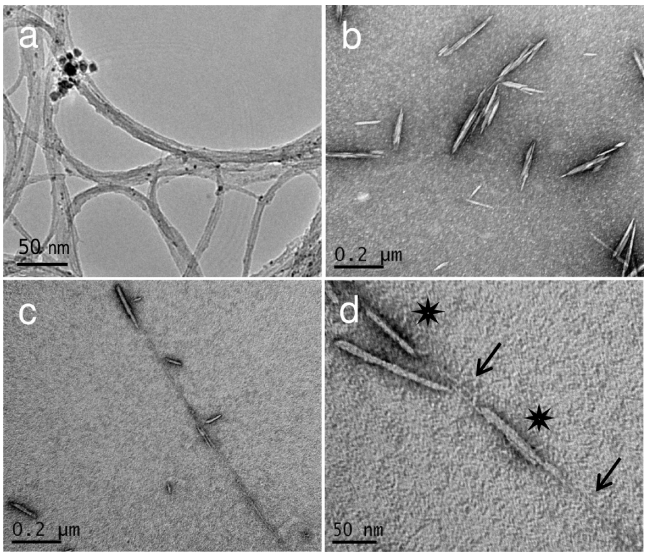

Figure 2. TEM images of (a) pristine SWNTs and (b) CN and (c, d) SWNT/CN morphology from a negatively stained diluted dispersion. (d) Short, thick objects are indicated by stars, and thinner, longer objects are indicated by arrows.

and from an SWNT/CN dispersion (Figure 2c,d). All of the images in Figure 2 are characteristic of our samples. The negatively stained CNs appear as elongated objects with a characteristic length of close to 200 nm. Both isolated and aggregated CNs are observed (Figure 2b). These observations agree with the results obtained by Elazzouzi et al.[22] that report an average CN length of 140 nm and a rectangular cross-section of approximately 6 × 6.1 nm × nm. Much longer objects are observed in the presence of SWNTs (Figures 2c,d). The length of these objects ranges from several hundred nanometers to several micrometers. Such lengths cannot be attributed to CNs. They correspond to the lengths usually observed for SWNTs. It can also be seen in Figure 2c that the thickness all along the object is not constant. At higher magnification, TEM images show very thin objects (indicated by arrows on Figure 2d) with thicknesses in the range of the nanometer, whereas in some other parts of the image, the objects are thicker (indicated by stars on Figure 2d), with thicknesses in the range of 10 nm. At first glance, the objects have lengths comparable to that of a nanotube, and the greater thickness is consistent with that of a CN. As a consequence, the formation of hybrid objects between CNs and SWNTs can be hypothesized. To investigate this hypothesis further, AFM images and height profile measurements along the object are displayed in Figure 3. (Figure 3a,b shows native CNs and SWNTs for comparison.) Typically, two kinds of profiles can be distinguished. The first one (height profiles 1 and 2, Figure 3c) corresponds to thin structures of about 1 nm in height (0.7 and 1.2 nm, respectively, for profiles 1 and 2). Such height values are lower than the CN thickness (typically 6 nm) but correspond instead to the diameter of an isolated SWNT or a very small bundle. The second type of profile reveals much thicker dimensions, as demonstrated by profiles 3 and 4 in Figure 3c (6 and 15 nm, respectively). These dimensions are in good agreement with the thickness of one or two CNs closely

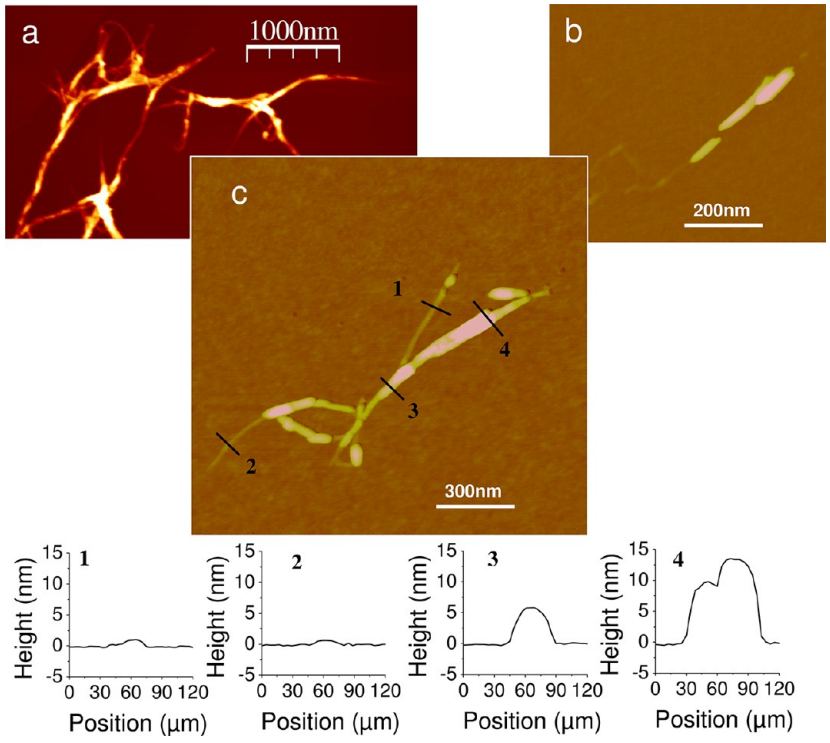

Figure 3. AFM height image of (a) pristine HiPco SWNTs (full-color *Z* scale = 50 nm), (b) CN, and (c) the SWNT/CN complex and associated height profiles. The full-color *Z* scale corresponds to 15 nm.

dx.doi.org/10.1021/la302077a | *Langmuir* 2012, 28, 12463−12471

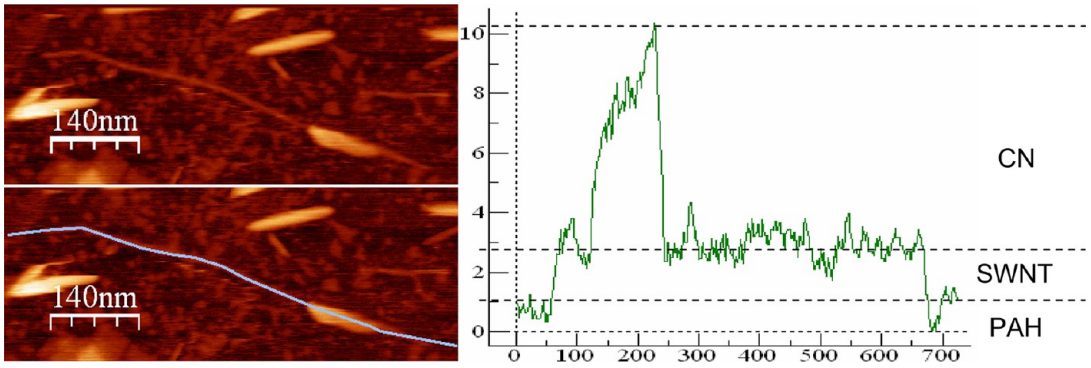

Figure 4. AFM height image obtained in water for an SWNT/CN complex and its associated height profile along the blue line. The full-color *Z* scale corresponds to 15 nm.

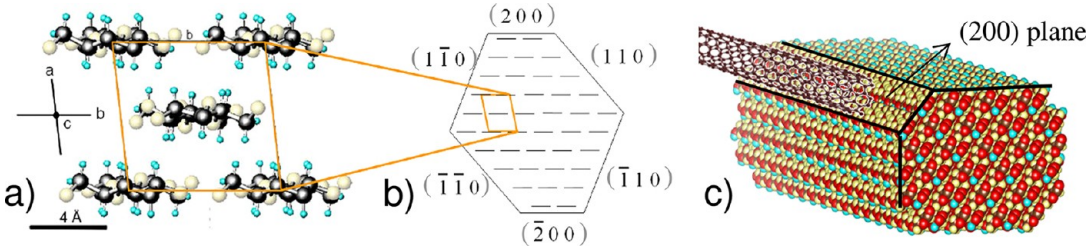

Figure 5. (a) Monoclinic unit cell and (b) schematic cross-section of cellulose nanocrystals. The (200) and ($\bar{2}$00) faces exhibit a higher hydrophobicity because of the exposure of CH moieties and are preferential sites for interaction with hydrophobic SWNTs. (c) Representation of a 6.5 SWNT near the (200) hydrophobic plane of a CN.

associated with the nanotubes. Thus, AFM and TEM images seem to indicate that the cellulose nanocrystals are aligned along the tube axis, with several CNs aligned along the same nanotube. To our knowledge, such a coalignment of a rodlike nanoparticle along a carbon nanotube has not been reported before. Because AFM and TEM images were obtained in a dry state, we cannot exclude the possibility at this stage that this alignment results from capillary forces pulling CNs to the SWNT surface during the drying step and that it does not correspond to the morphology of the SWNT/CN hybrids in the dispersion. To probe the morphology of the hybrids in the wet state and to avoid a possible effect of capillary forces, AFM images were obtained in ultrapure water on wet samples prepared without the drying step. One of these images is displayed in Figure 4. This image is very close to the image in Figure 3c. A 700-nm-long filament object is observed with an average thickness of 1.8 nm, corresponding to a bundle of two or three SWNTs. A shorter and thicker particle, with a thickness of about 8 nm, overlaps the first one and can be identified as a CN. This result therefore shows that the CN self-aligns along the SWNT, even in the wet state. We can also conclude that capillary forces are not the driving forces for association. The self-assembly process might result from the surface properties of CNs and SWNTs.

Several biopolymers, including proteins[46] and polysaccharides,[47] have been identified as dispersants of SWNTs. The stabilization mechanisms that have been proposed include wrapping the polymer around the tube,[48] hydrophobic interactions between the hydrophobic carbon surface and hydrophobic segments of the chains,[49] and CH−π interactions.[50] CNs are rigid rods of crystalline cellulose for which a wrapping mechanism is obviously not conceivable. An important issue that has to be taken into account to explain the CN/SWNT interaction is the hydrophobicity of the CNs. The crystalline native phases, referred to as cellulose Iα and Iβ, are dense intra- and intermolecular H-bond networks that induce the orientation of functional groups. This leads to a highly ordered crystalline structure that exposes planes with different chemical characteristics. A schematic cross-section of cellulose nanocrystals is given in Figure 5. Recent molecular dynamics calculations[51] have shown that cellulose nanocrystal faces can be divided into three different families. Two families that differ by their roughness exhibit hydrophilic characteristics because of the preferential exposure of the hydroxyl group. The last type of surface ((200) planes of the monoclinic cell, see Figure 5) displays hydrophobic character because C−H moieties are predominant. The hydrophobic character on some CN faces was experimentally demonstrated by Lethio et al.,[52] who reported the specific binding of hydrophobic cellulose binding modules on the hydrophobic faces of CNs. The ability of CNs to stabilize oil-in-water Pickering emulsions[53] is also attributed to the hydrophobic character of some CN faces. Because the graphitic surface of the single-walled nanotubes is hydrophobic, hydrophobic interactions between the SWNT surface and the hydrophobic (200) CN planes are likely to occur (Figure 5). Figure 5c is a representation of the 1β lattice expected for cotton nanocrystals with lateral dimensions of 6 nm × 6 nm, in agreement with the dimensions reported earlier.[22] Hydrophobic interactions between SWNTs and amphiphilic species such as surfactants (SDS, SC, etc.),[54] peptides,[55] and block copolymers[56] have already been reported. In the SWNT/CN hybrids, it can be suggested that the hydrophobic faces of the CNs can interact with hydrophobic SWNTs by expelling water and thus stabilizing the dispersion of the SWNTs. Because the hydrophobic surfaces of the CNs represent only a part of the CN surfaces, it should result in the formation of an SWNT/CN complex where the CNs would be aligned along the nanotube

dx.doi.org/10.1021/la302077a | *Langmuir* 2012, 28, 12463−12471

long axis. Although hydrophobic interactions are the driving forces for the association mechanism between SWNTs and CNs, long-range electrostatic repulsion also plays a role in the stabilization of the SWNT/CN dispersion. This electrostatic repulsion between the CNs may limit the number of CNs associated with SWNTs in the hybrid architecture. As shown in Figures 2 and 3, the SWNT surface is not fully covered with CNs despite an [SWNT]/[CN] ratio of 0.0028. This thus ensures the repulsion of the CN/SWNT hybrids, allowing them to remain dispersed in water without aggregation and further precipitation. As a result of the rigid nanorod-specific shape and interaction capabilities of CNs, the development of such new hybrids leads to opportunities for the creation of new nanomaterials. For example, the polyelectrolyte nature of CNs makes it possible to incorporate these SWNT/CN hybrids in LbL thin films.

c. SWNT/CN Films. Since LbL self-assembled multilayered thin films made of CNs were first prepared in 2005,[17] the growth pattern, structure, and properties of multilayered films that incorporate CNs have been studied[57] in relation to their processing parameters, including the polyelectrolyte nature, the effect of ionic strength, and the method of deposition (e.g., spin coating, dipping).[23,58−62] These previous papers report interesting optical properties of the films that have found applications in antireflective coatings[8] and enzyme detection.[20] In our study, LbL CN-based films were prepared using the dipping technique, consisting of the alternate immersion of the substrate in cationic PAH solution and anionic SWNT/CN dispersion or a pure CN suspension as reference samples. Figure 6 displays the thickness of each film, measured by

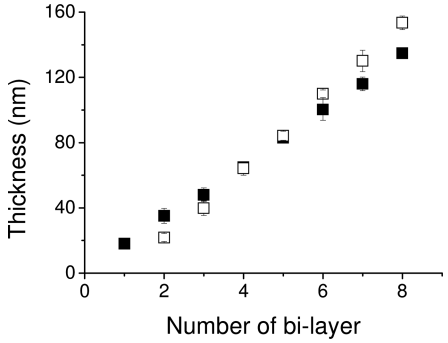

Figure 6. Thickness of PAH−CNs (□) and PAH-SWNTs/CNs (■) multilayered LBL films vs the number of bilayer depositions. Each data point represents the average of six measurements, with deviations shown by error bars. In some cases, the error bars are smaller than the symbols.

profilometry, as a function of the bilayer number. Homogeneous films with low roughness were obtained, as demonstrated by small error bars reflecting six different measurements obtained for each thickness value. The unfilled squares represent the data obtained for the growth of the CN dispersion alone. The growth pattern shows that the thickness of the films increases linearly with the number of bilayers. The slope of the growth pattern is found to be 18 nm/bilayer. Because the PAH layer is less than 2 nm thick,[63] the bilayer thickness is mainly dominated by the thickness of the CNs with or without SWNTs. It should be recalled here that the CNs have a typical thickness of 6 to 7 nm. A bilayer thickness of 18 nm thus suggests that the CNs are incorporated into the films as double layers, as previously reported by Jean et al.[57] who found a bilayer thickness of approximately 16 nm for dipped LbL PAH−CN films. The adsorption of a double layer of CNs for each PAH/CN bilayer is attributed to the weak surface charge density of CNs versus that of PAHs and to the conformation of the PAH chains that adsorb on the surface in a random coil conformation.[64] The black (filled) points show the growth pattern obtained with the SWNT/CN dispersion. This growth pattern is characterized by a 17 nm bilayer slope that is identical to the one obtained without SWNTs. This indicates that film growth occurs linearly whether the SWNTs are present or not. It also shows that the SWNT/CN interaction does not significantly affect the adsorption process and the film growth.

The presence of SWNTs in the films has to be checked. Raman scattering spectroscopy with excitation at 1064 nm is a good tool for probing for the presence of SWNTs. As shown in Figure 7, PAH/CN films without SWNTs (thin line) do not

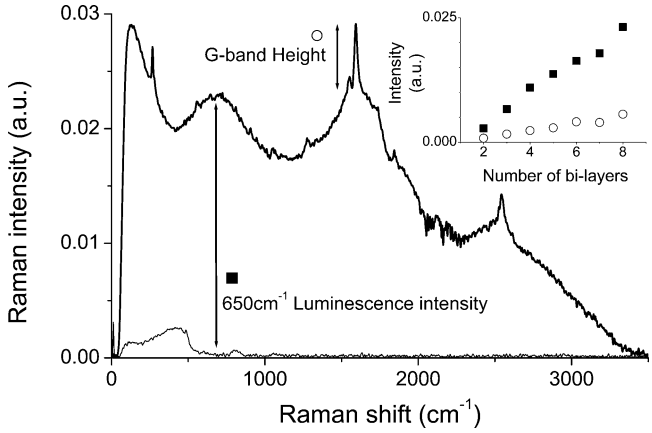

Figure 7. Raman spectra of eight bilayer films obtained from a CN suspension (thin line) and SWNT/CN dispersions (bold line) obtained at an excitation wavelength of 1064 nm. (Inset) Evolution of the G band (○) and luminescence intensities (■) vs the number of bilayer depositions. The luminescence intensity is extracted without baseline subtraction and is representative of the global luminescence of the samples, whereas G-band intensities are obtained after the elimination of the luminescence signal as illustrated by the arrows.

show any significant Raman signal, except the one corresponding to the quartz substrate in the 100−500 cm^{-1} range. Conversely, a nice Raman signal can be obtained from the films prepared from SWNT/CN dispersions (bold line). These spectra exhibit the characteristic Raman signature of SWNTs (i.e., radial breathing mode (RBM) bands close to 260 cm^{-1} and a tangential mode (G bands) at approximately 1590 cm^{-1}). Because each layer is adsorbed from the same initial SWNT/CN dispersion and thanks to our experimental equipment, SWNTs are under the same resonance conditions in each layer. Thus, Raman scattering intensities can be compared and used for relative quantitative characterization. The growth of the G-band signal has been monitored versus the number of deposited bilayers. The result is shown in the inset of Figure 7: the G-band intensity increases linearly with the number of bilayers. It unambiguously shows that a constant number of SWNTs are incorporated into each adsorbed CN layer. Indeed, it is probable that they are incorporated as SWNT/CN hybrids.

More surprisingly, SWNT/CN films exhibit a significant NIR luminescence signal (broad bands located at Raman shifts of 650 and 1650 cm^{-1}). These luminescence bands correspond to

dx.doi.org/10.1021/la302077a | Langmuir 2012, 28, 12463−12471

the luminescence peaks of Figure 1 at 1150 and 1300 nm. As shown in the inset of Figure 7, the luminescence signal also increases linearly with the number of bilayers. The fact that the luminescence of the SWNTs is preserved in the solid state (i.e., in the film) is quite unusual. As already mentioned, NIR luminescence of a semiconducting SWNT is quenched when the semiconducting nanotubes are in the vicinity of metallic nanotubes.[44] This therefore implies that well-isolated SWNTs have been incorporated into the films. It also suggests that the previously described SWNT/CN hybrid structure obtained by the dispersion process is preserved during the adsorption step and the formation of the solid film.

The presence of SWNTs in the films is also confirmed by SEM micrographs. Figure 8a,b shows SEM images of the surface of an SWNT/CN eight-bilayer film obtained with and without metallization, respectively. Similar images have been obtained from one and two bilayer films (Supporting Information). These types of SEM experiments with or without metallization are a classical way to identify conducting fillers in an insulating matrix. Because the CNs are insulators, metallization is mandatory to avoid charging effects and to obtain well-resolved SEM micrographs. Figure 8a, obtained after metallization, clearly shows the cellulose nanocrystals, whereas SWNTs are not observed in this image because they are too thin. Conversely, on Figure 8b where no metallization was used, the CNs are not observed but a loose network of long and white filaments that are probably the conducting nanotubes[65] can be observed. Indeed, it has been checked that SEM of a pure CN film without metallization gives a uniformly gray image (Supporting Information). It is interesting that the SWNT network appears to be percolating through the image and, therefore, that the film may be electrically conductive.

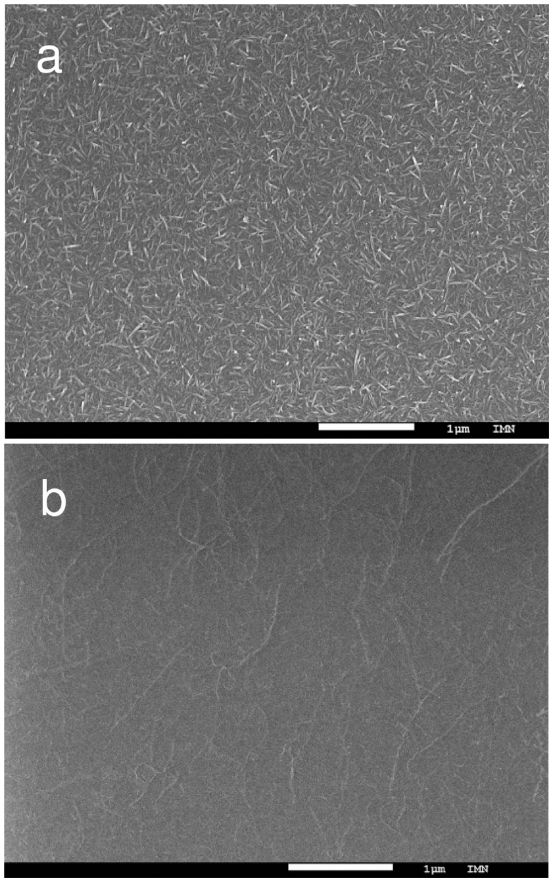

Figure 8. SEM micrographs of eight-bilayer PAH-SWNT/CN films: (a) obtained with preliminary metallization of the surface; (b) obtained without metallization. The CN crystals are easily seen in panel a, and the SWNTs are revealed in panel b. Scale bars (white) = 1 μm.

4. CONCLUSIONS

This article shows that it is possible to disperse SWNTs in a CN colloidal suspension. Stable, highly concentrated dispersions were obtained using a noncovalent functionalization method. SWNTs and CNs self-assemble in hybrids characterized by the alignment of several CNs along the SWNT axis. We argue that short-range hydrophobic interactions occur between the SWNTs and specific crystalline faces of the CNs, which are responsible for this specific architecture. Long-range electrostatic repulsion between the CNs also plays a role in the stabilization of the SWNT/CN dispersion.

When these dispersions are used, it is possible to grow LbL films with a controlled thickness depending on the number of bilayers. In this article, we reported the growth of PAH-SWNT/CN bilayers with an average thickness per bilayer of approximately 17 nm. This thickness corresponds to a double layer of cellulose nanocrystals. The SWNTs are incorporated into each layer as shown by Raman scattering spectroscopy and SEM micrographs. The layered structure of the films leads to an in-plane alignment of cellulose nanocrystals and, as a result, SWNTs. It is worth noting that the films exhibit an NIR luminescence signal arising from the luminescence of isolated semiconducting SWNTs. This result is quite unusual and attests to the specificity of these hybrid-based LbL films. Because the luminescence of the SWNTs is highly dependent on the local environment, this property may open the way to sensing applications of the films.

The composition, structure, and properties of such LbL multilayered thin films can be modulated by varying the SWNT/CN ratio, the nature of the polyelectrolytes, and the deposition conditions. We therefore expect to be able to build multifunctional nanocomposite films with unique properties using cellulose and SWNTs.

■ ASSOCIATED CONTENT

Ⓢ Supporting Information

SEM images of one- and two-bilayer PAH-SWNT-CN films and an eight-bilayer PAH−CN film. This material is available free of charge via the Internet at http://pubs.acs.org.

■ AUTHOR INFORMATION

Corresponding Author

*Tel: +33 (0)2 40 37 39 86. Fax: +33 (0)2 40 37 39 91. E-mail: christophe.olivier@cnrs-imn.fr.

Notes

The authors declare no competing financial interest.

■ ACKNOWLEDGMENTS

This work was partially supported by the French Pays de Loire Regional Council through the NANOFONC program. We gratefully acknowledge Nicolas Gautier from IMN (Institut des Matériaux de Nantes) for TEM pictures of pristine SWNTs.

REFERENCES

(1) Ulman, A. Formation and Structure of Self-Assembled Monolayers. *Chem. Rev.* **1996**, *96*, 1533−1554.

(2) Zasadzinski, J. A.; Viswanathan, R.; Madsen, L.; Garnaes, J.; Schwartz, D. K. Langmuir-Blodgett Films. *Science* **1994**, *263*, 1726−1733.

(3) Decher, G.; Hong, J. D.; Schmitt, J. Buildup of Ultrathin Multilayer Films by a Self-Assembly Process: III. Consecutively Alternating Adsorption of Anionic and Cationic Polyelectrolytes on Charged Surfaces. *Thin Solid Films* **1992**, *210−211*, 831−835.

(4) Li, H.; Pang, S.; Wu, S.; Feng, X.; Mullen, K.; Bubeck, C. Layer-by-Layer Assembly and UV Photoreduction of Graphene Polyoxometalate Composite Films for Electronics. *J. Am. Chem. Soc.* **2011**, *133*, 9423−9429.

(5) Ariga, K.; Nakanishi, T.; Michinobu, T. Immobilization of Biomaterials to Nano-Assembled Films (Self-Assembled Monolayers, Langmuir-Blodgett Films, and Layer-by-Layer Assemblies) and Their Related Functions. *J. Nanosci. Nanotechnol.* **2006**, *6*, 2278−2301.

(6) Hammond, P. T. Form and Function in Multilayer Assembly: New Applications at the Nanoscale. *Adv. Mater.* **2004**, *16*, 1271−1293.

(7) Dubas, S. T.; Schlenoff, J. B. Factors Controlling the Growth of Polyelectrolyte Multilayers. *Macromolecules* **1999**, *32*, 8153−8160.

(8) Podsiadlo, P.; Sui, L.; Elkasabi, Y.; Burgardt, P.; Lee, J.; Miryala, A.; Kusumaatmaja, W.; Carman, M. R.; Shtein, M.; Kieffer, J.; Lahann, J.; Kotov, N. A. Layer-by-Layer Assembled Films of Cellulose Nanowires with Antireflective Properties. *Langmuir* **2007**, *23*, 7901−7906.

(9) Decher, G.; Schmitt, J. Fine-Tuning of the Film Thickness of Ultrathin Multilayer Films Composed of Consecutively Alternating Layers of Anionic and Cationic Polyelectrolytes. In *Trends in Colloid and Interface Science VI*; Helm, C., Lösche, M., Möhwald, H., Eds.; Springer-Verlag: New York, 1992; Vol. *89*, pp 160−164.

(10) Fou, A. C.; Onitsuka, O.; Ferreira, M.; Rubner, M. F.; Hsieh, B. R. Fabrication and Properties of Light-Emitting Diodes Based on Self-Assembled Multilayers of Poly(Phenylene Vinylene). *J. Appl. Phys.* **1996**, *79*, 7501−7509.

(11) Lvov, Y.; Yamada, S.; Kunitake, T. Non-Linear Optical Effects in Layer-by-Layer Alternate Films of Polycations and an Azobenzene-Containing Polyanion. *Thin Solid Films* **1997**, *300*, 107−112.

(12) Wood, K. C.; Boedicker, J. Q.; Lynn, D. M.; Hammond, P. T. Tunable Drug Release from Hydrolytically Degradable Layer-by-Layer Thin Films. *Langmuir* **2005**, *21*, 1603−1609.

(13) Ferreira, M.; Fiorito, P. A.; Oliveira, O. N., Jr; Cordoba de Torresi, S. I. Enzyme-Mediated Amperometric Biosensors Prepared with the Layer-by-Layer (LbL) Adsorption Technique. *Biosens. Bioelectron.* **2004**, *19*, 1611−1615.

(14) Kotov, N. A.; Dekany, I.; Fendler, J. H. Layer-by-Layer Self-Assembly of Polyelectrolyte-Semiconductor Nanoparticle Composite Films. *J. Phys. Chem.* **1995**, *99*, 13065−13069.

(15) Mamedov, A. A.; Kotov, N. A.; Prato, M.; Guldi, D. M.; Wicksted, J. P.; Hirsch, A. Molecular Design of Strong Single-Wall Carbon Nanotube/Polyelectrolyte Multilayer Composites. *Nat. Mater.* **2002**, *1*, 190−194.

(16) Mamedov, A.; Ostrander, J.; Aliev, F.; Kotov, N. A. Stratified Assemblies of Magnetite Nanoparticles and Montmorillonite Prepared by the Layer-by-Layer Assembly. *Langmuir* **2000**, *16*, 3941−3949.

(17) Podsiadlo, P.; Choi, S.-Y.; Shim, B.; Lee, J.; Cuddihy, M.; Kotov, N. A. Molecularly Engineered Nanocomposites: Layer-by-Layer Assembly of Cellulose Nanocrystals. *Biomacromolecules* **2005**, *6*, 2914−2918.

(18) Podsiadlo, P.; Kaushik, A. K.; Arruda, E. M.; Waas, A. M.; Shim, B. S.; Xu, J.; Nandivada, H.; Pumplin, B. G.; Lahann, J.; Ramamoorthy, A.; Kotov, N. A. Ultrastrong and Stiff Layered Polymer Nanocomposites. *Science* **2007**, *318*, 80−83.

(19) Valentin, R.; Cerclier, C.; Geneix, N.; Aguié-Béghin, V.; Gaillard, C. d.; Ralet, M.-C.; Cathala, B. Elaboration of Extensin-Pectin Thin Film Model of Primary Plant Cell Wall. *Langmuir* **2010**, *26*, 9891−9898.

(20) Cerclier, C.; Guyomard-Lack, A.; Moreau, C.; Cousin, F.; Beury, N.; Bonnin, E.; Jean, B.; Cathala, B. Coloured Semi-reflective Thin Films for Biomass-Hydrolyzing Enzyme Detection. *Adv. Mater.* **2011**, *23*, 3791−3795.

(21) Eichhorn, S. J. Cellulose Nanowhiskers: Promising Materials for Advanced Applications. *Soft Matter* **2011**, *7*, 303−315.

(22) Elazzouzi-Hafraoui, S.; Nishiyama, Y.; Putaux, J.-L.; Heux, L.; Dubreuil, F.; Rochas, C. The Shape and Size Distribution of Crystalline Nanoparticles Prepared by Acid Hydrolysis of Native Cellulose. *Biomacromolecules* **2007**, *9*, 57−65.

(23) Cranston, E. D.; Gray, D. G. Morphological and Optical Characterization of Polyelectrolyte Multilayers Incorporating Nanocrystalline Cellulose. *Biomacromolecules* **2006**, *7*, 2522−2530.

(24) Wagberg, L.; Decher, G.; Norgren, M.; Lindstrom, T.; Ankerfors, M.; Axnas, K. The Build-Up of Polyelectrolyte Multilayers of Microfibrillated Cellulose and Cationic Polyelectrolytes. *Langmuir* **2008**, *24*, 784−795.

(25) Cerclier, C.; Cousin, F.; Bizot, H.; Moreau, C. l.; Cathala, B. Elaboration of Spin-Coated Cellulose-Xyloglucan Multilayered Thin Films. *Langmuir* **2010**, *26*, 17248−17255.

(26) Popov, V. N. Carbon Nanotubes: Properties and Application. *Mater. Sci. Eng., R* **2004**, *43*, 61−102.

(27) Kovtyukhova, N. I.; Mallouk, T. E.; Pan, L.; Dickey, E. C. Individual Single-Walled Nanotubes and Hydrogels Made by Oxidative Exfoliation of Carbon Nanotube Ropes. *J. Am. Chem. Soc.* **2003**, *125*, 9761−9769.

(28) Pompeo, F.; Resasco, D. E. Water Solubilization of Single-Walled Carbon Nanotubes by Functionalization with Glucosamine. *Nano Lett.* **2002**, *2*, 369−373.

(29) Zhao, J.; Park, H.; Han, J.; Lu, J. P. Electronic Properties of Carbon Nanotubes with Covalent Sidewall Functionalization. *J. Phys. Chem. B* **2004**, *108*, 4227−4230.

(30) Backes, C.; Hirsch, A. Noncovalent Functionalization of Carbon Nanotubes. In *Chemistry of Nanocarbons*; Akasaka, T., Wudl, F., Nagase, S., Eds.; John Wiley & Sons: Chichester, U.K., 2010; pp 1−48.

(31) Zhang, X.; Liu, T.; Sreekumar, T. V.; Kumar, S.; Moore, V. C.; Hauge, R. H.; Smalley, R. E. Poly(vinyl alcohol)/SWNT Composite Film. *Nano Lett.* **2003**, *3*, 1285−1288.

(32) Zhu, J.; Shim, B. S.; Di Prima, M.; Kotov, N. A. Transparent Conductors from Carbon Nanotubes LBL-Assembled with Polymer Dopant with $\pi-\pi$ Electron Transfer. *J. Am. Chem. Soc.* **2011**, *133*, 7450−7460.

(33) Rahman, G. M. A.; Guldi, D. M.; Cagnoli, R.; Mucci, A.; Schenetti, L.; Vaccari, L.; Prato, M. Combining Single Wall Carbon Nanotubes and Photoactive Polymers for Photoconversion. *J. Am. Chem. Soc.* **2005**, *127*, 10051−10057.

(34) Loh, K. J.; Kim, J.; Lynch, J. P.; Nadine Wong Shi, K.; Kotov, N. A. Multifunctional Layer-by-Layer Carbon Nanotube Polyelectrolyte Thin Films for Strain and Corrosion Sensing. *Smart Mater. Struct.* **2007**, *16*, 429−438.

(35) Tsai, T.-W.; Heckert, G.; Neves, L. s. F.; Tan, Y.; Kao, D.-Y.; Harrison, R. G.; Resasco, D. E.; Schmidtke, D. W. Adsorption of Glucose Oxidase onto Single-Walled Carbon Nanotubes and Its Application in Layer-By-Layer Biosensors. *Anal. Chem.* **2009**, *81*, 7917−7925.

(36) Nepal, D.; Balasubramanian, S.; Simonian, A. L.; Davis, V. A. Strong Antimicrobial Coatings: Single-Walled Carbon Nanotubes Armored with Biopolymers. *Nano Lett.* **2008**, *8*, 1896−1901.

(37) Qichao, Z.; Xunda, F.; Shilin, M.; Zhaoxia, J. Carbon-Nanotube-Assisted High Loading and Controlled Release of Polyoxometalates in Biodegradable Multilayer Thin Films. *Nanotechnology* **2009**, *20*, 105101.

(38) Dong, X. M.; Revol, J. F.; Gray, D. G. Effect of Microcrystallite Preparation Conditions on the Formation of Colloid Crystals of Cellulose. *Cellulose* **1998**, *5*, 19−32.

(39) Horcas, I.; Fernandez, R.; Gomez-Rodriguez, J. M.; Colchero, J.; Gomez-Herrero, J.; Baro, A. M. WSXM: A Software for Scanning Probe Microscopy and a Tool for Nanotechnology. *Rev. Sci. Instrum.* **2007**, *78*, 013705−013708.

(40) Shim, B. S.; Kotov, N. A. Single-Walled Carbon Nanotube Combing during Layer-by-Layer Assembly: From Random Adsorption to Aligned Composites. *Langmuir* **2005**, *21*, 9381−9385.
(41) Ishibashi, A.; Yamaguchi, Y.; Murakami, H.; Nakashima, N. Layer-by-Layer Assembly of RNA/Single-Walled Carbon Nanotube Nanocomposites. *Chem. Phys. Lett.* **2006**, *419*, 574−577.
(42) Haggenmueller, R.; Rahatekar, S. S.; Fagan, J. A.; Chun, J.; Becker, M. L.; Naik, R. R.; Krauss, T.; Carlson, L.; Kadla, J. F.; Trulove, P. C.; Fox, D. F.; DeLong, H. C.; Fang, Z.; Kelley, S. O.; Gilman, J. W. Comparison of the Quality of Aqueous Dispersions of Single Wall Carbon Nanotubes Using Surfactants and Biomolecules. *Langmuir* **2008**, *24*, 5070−5078.
(43) Saito, R.; Dresselhaus, G.; Dresselhaus, M. S. *Physical Properties of Carbon Nanotubes*; Imperial College Press: 1998.
(44) O'Connell, M. J.; Bachilo, S. M.; Huffman, C. B.; Moore, V. C.; Strano, M. S.; Haroz, E. H.; Rialon, K. L.; Boul, P. J.; Noon, W. H.; Kittrell, C.; Ma, J.; Hauge, R. H.; Weisman, R. B.; Smalley, R. E. Band Gap Fluorescence from Individual Single-Walled Carbon Nanotubes. *Science* **2002**, *297*, 593−596.
(45) Bachilo, S. M.; Strano, M. S.; Kittrell, C.; Hauge, R. H.; Smalley, R. E.; Weisman, R. B. Structure-Assigned Optical Spectra of Single-Walled Carbon Nanotubes. *Science* **2002**, *298*, 2361−2366.
(46) Karajanagi, S. S.; Yang, H.; Asuri, P.; Sellitto, E.; Dordick, J. S.; Kane, R. S. Protein-Assisted Solubilization of Single-Walled Carbon Nanotubes. *Langmuir* **2006**, *22*, 1392−1395.
(47) Riou, I.; Bertoncini, P.; Bizot, H.; Mevellec, J. Y.; Buléon, A.; Chauvet, O. Carboxymethylcellulose/Single Walled Carbon Nanotube Complexes. *J. Nanosci. Nanotechnol.* **2009**, *9*, 6176−6180.
(48) Minami, N.; Kim, Y.; Miyashita, K.; Kazaoui, S.; Nalini, B. Cellulose Derivatives as Excellent Dispersants for Single-Wall Carbon Nanotubes as Demonstrated by Absorption and Photoluminescence Spectroscopy. *Appl. Phys. Lett.* **2006**, *88*, 093123−.
(49) Erlanger, B. F.; Chen, B.-X.; Zhu, M.; Brus, L. Binding of an Anti-Fullerene IgG Monoclonal Antibody to Single Wall Carbon Nanotubes. *Nano Lett.* **2001**, *1*, 465−467.
(50) Zheng, M.; Jagota, A.; Semke, E. D.; Diner, B. A.; McLean, R. S.; Lustig, S. R.; Richardson, R. E.; Tassi, N. G. DNA-Assisted Dispersion and Separation of Carbon Nanotubes. *Nat. Mater.* **2003**, *2*, 338−342.
(51) Mazeau, K. On the External Morphology of Native Cellulose Microfibrils. *Carbohydr. Polym.* **2011**, *84*, 524−532.
(52) Lehtio, J.; Sugiyama, J.; Gustavsson, M.; Fransson, L.; Linder, M.; Teeri, T. T. The Binding Specificity and Affinity Determinants of Family 1 and Family 3 Cellulose Binding Modules. *Proc. Natl. Acad. Sci. U.S.A.* **2003**, *100*, 484−489.
(53) Kalashnikova, I.; Bizot, H.; Cathala, B.; Capron, I. New Pickering Emulsions Stabilized by Bacterial Cellulose Nanocrystals. *Langmuir* **2011**, *27*, 7471−7479.
(54) Vigolo, B.; Pénicaud, A.; Coulon, C.; Sauder, C. d.; Pailler, R.; Journet, C.; Bernier, P.; Poulin, P. Macroscopic Fibers and Ribbons of Oriented Carbon Nanotubes. *Science* **2000**, *290*, 1331−1334.
(55) Dieckmann, G. R.; Dalton, A. B.; Johnson, P. A.; Razal, J.; Chen, J.; Giordano, G. M.; Munoz, E.; Musselman, I. H.; Baughman, R. H.; Draper, R. K. Controlled Assembly of Carbon Nanotubes by Designed Amphiphilic Peptide Helices. *J. Am. Chem. Soc.* **2003**, *125*, 1770−1777.
(56) Shin, H.-i.; Min, B. G.; Jeong, W.; Park, C. Amphiphilic Block Copolymer Micelles: New Dispersant for Single Wall Carbon Nanotubes. *Macromol. Rapid Commun.* **2005**, *26*, 1451−1457.
(57) Jean, B.; Dubreuil, F.; Heux, L.; Cousin, F. Structural Details of Cellulose Nanocrystals/Polyelectrolytes Multilayers Probed by Neutron Reflectivity and AFM. *Langmuir* **2008**, *24*, 3452−3458.
(58) Cranston, E. D.; Gray, D. G. Birefringence in Spin-Coated Films Containing Cellulose Nanocrystals. *Colloids Surf., A* **2008**, *325*, 44−51.
(59) Sui, L.; Huang, L.; Podsiadlo, P.; Kotov, N. A.; Kieffer, J. Brillouin Light Scattering Investigation of the Mechanical Properties of Layer-by-Layer Assembled Cellulose Nanocrystal Films. *Macromolecules* **2010**, *43*, 9541−9548.
(60) Cranston, E. D.; Gray, D. G.; Rutland, M. W. Direct Surface Force Measurements of Polyelectrolyte Multilayer Films Containing Nanocrystalline Cellulose. *Langmuir* **2010**, *26*, 17190−17197.
(61) de Mesquita, J. P.; Donnici, C. L.; Pereira, F. V. Biobased Nanocomposites from Layer-by-Layer Assembly of Cellulose Nanowhiskers with Chitosan. *Biomacromolecules* **2010**, *11*, 473−480.
(62) de Mesquita, J. P.; Patricio, P. S.; Donnici, C. L.; Petri, D. F. S.; de Oliveira, L. C. A.; Pereira, F. V. Hybrid Layer-by-Layer Assembly Based on Animal and Vegetable Structural Materials: Multilayered Films of Collagen and Cellulose Nanowhiskers. *Soft Matter* **2011**, *7*, 4405−4413.
(63) Schmitt, J.; Gruenewald, T.; Decher, G.; Pershan, P. S.; Kjaer, K.; Loesche, M. Internal Structure of Layer-by-Layer Adsorbed Polyelectrolyte Films: A Neutron and X-ray Reflectivity Study. *Macromolecules* **1993**, *26*, 7058−7063.
(64) Moreau, C.; Beury, N.; Delorme, N.; Cathala, B. Tuning the Architecture of Cellulose Nanocrystals-Poly(Allylamine Hydrochloride) Multilayered Thin Films: Influence of Dipping Parameters. *Langmuir* **2012**, *28*, 10425−10436.
(65) Loos, J.; Alexeev, A.; Grossiord, N.; Koning, C. E.; Regev, O. Visualization of Single-Wall Carbon Nanotube (SWNT) Networks in Conductive Polystyrene Nanocomposites by Charge Contrast Imaging. *Ultramicroscopy* **2005**, *104*, 160−167.